Supporting Information Appendix

Quantitative nanoscale imaging of orientational order in biological filaments by polarized super-resolution microscopy, by Cesar Augusto Valades Cruz et al.

Supporting Information Note 1. Model

A single molecule orientation is determined by its absorption dipole $\vec{\mu}_a(\theta_a, \varphi_a)$ and emission dipole $\vec{\mu}_e(\theta_e, \varphi_e)$, which lie along transition dipole moment directions for the respective absorption and emission transitions. The dipoles orientations (θ_a, φ_a) and (θ_e, φ_e) are defined in the (X,Y,Z) frame, (X,Y) being the sample plane and (Z) the propagation direction (Fig. 1a). For a stationary molecule (e.g. no time dependence of its orientation during the integration time of the detector), and for a plane wave propagation (low excitation/collection aperture), the fluorescence intensities radiated along the X and Y polarization directions, are deduced from the absorption and emission probabilities product[1–3]:

$$I_X(\theta_a, \varphi_a, \theta_e, \varphi_e) = \left|\vec{\mu}_a(\theta_a, \varphi_a) \cdot \vec{E}\right|^2 \left|\vec{\mu}_e(\theta_e, \varphi_e) \cdot \vec{X}\right|^2$$
$$I_Y(\theta_a, \varphi_a, \theta_e, \varphi_e) = \left|\vec{\mu}_a(\theta_a, \varphi_a) \cdot \vec{E}\right|^2 \left|\vec{\mu}_e(\theta_e, \varphi_e) \cdot \vec{Y}\right|^2$$

Here and in what follows, "=" encompasses all collection/excitation efficiency factors that do not affect the present analysis. Under incident circular excitation, at normal incidence, the photo-selection of Z contribution of the absorption dipole is very low, and homogeneous in the (X,Y) plane. The fluorescence intensities can be simplified since there is no polarized photo-selection at the excitation step:

$$I_X(\theta, \varphi) = \left|\vec{\mu}_e(\theta, \varphi) \cdot \vec{X}\right|^2 \text{ and } I_Y(\theta, \varphi) = \left|\vec{\mu}_e(\theta, \varphi) \cdot \vec{Y}\right|^2$$

where (θ_e, φ_e) is replaced by (θ, φ) in what follows, for simplicity.

The high numerical aperture (NA) of the collection objective mixes propagation directions and therefore polarization directions. Intensities measured after the detection microscope objective, in both X (called ∥ under high NA) and Y (called ⊥ under high NA) polarization direction are[4]:

$$I_{\parallel}(\theta, \varphi) = \kappa_1 I_X(\theta, \varphi) + \kappa_2 I_Y(\theta, \varphi) + \kappa_3 I_Z(\theta, \varphi)$$
$$I_{\perp}(\theta, \varphi) = \kappa_1 I_Y(\theta, \varphi) + \kappa_2 I_X(\theta, \varphi) + \kappa_3 I_Z(\theta, \varphi)$$

Where the $(\kappa_1, \kappa_2, \kappa_3)$ coefficients depend on NA, following [4]. In the present situation with NA = 1.3 using an oil immersion objective: $\kappa_1 = 0.781, \kappa_2 = 0.01, \kappa_3 = 0.209$.

We define the total intensity collected for one molecule by

$$I_T(\theta,\varphi) = I_{\parallel}(\theta,\varphi) + I_{\perp}(\theta,\varphi)$$

And the polarization factor by:

$$P = \frac{I_{\parallel} - I_{\perp}}{I_{\parallel} + I_{\perp}}$$

For a stationary molecule in the case of a low NA collection, the orientation angle of the molecule in the sample plane (φ) can be directly related to P, independently from its out-of-plane orientation θ, following the relation:

$$P = \cos(2\varphi)$$

And therefore the single molecule in-plane direction is directly deduced from the measurement of P by: $\varphi = \frac{1}{2} acosP$. Note that this relations implies an ambiguity of determination between φ and $\pi - \varphi$ that cannot be waived unless more polarization states are detected[2].

Generally single molecules are not completely fixed in orientation and rotational diffusion occurs. We account therefore for a possible molecular angle wobbling of $\vec{\mu}_e(\theta,\varphi)$, within a cone aperture of angular range δ and average pointing direction (ρ,η) (Fig. 1b). If the rotation time is faster than the integration time of the measurement, averaged quantities have to be considered instead of the stationary expressions above. Note that since the excitation is circularly polarized, no specific photo-selection orientation is induced in the sample plane, and thus the relative strength between rotational time and fluorescence life time does not matter, as long as both fluorescence life time and rotational times are much faster than the integration time (which is generally the case). In contrast, traditional anisotropy measurements that use linear excitation are dependent on the ratio (fluorescence lifetime/ rotation time).
The measured intensities along the X and Y polarizations are written now as the sum over all explored orientation angles during the integration time T. Supposing that these angles are confined in an angular cone aperture δ:

$$I_X = \int_0^{2\pi} d\varphi \int_0^{\pi} d\theta \ \sin\theta \left|\vec{\mu}_e(\theta,\varphi,\rho,\eta)\cdot\vec{X}\right|^2 f(\theta,\varphi)$$

And similarly for I_Y. $f(\theta,\varphi)$ is a cone function, of value 1 for ($\theta < \delta/2$) and 0 elsewhere (a Gaussian function would not change the results significantly). ρ is the orientation of the projection of the cone in the sample plane (X,Y), and η is the out-of-plane orientation of the cone, relative to Z (Fig. 1b).

We consider here molecular order within a biological fiber lying in the (X,Y) plane, made of filaments which follow a main macroscopic direction ρ_{av} (with respect to X) (Fig. 1b). Each fluorophore (= single molecule emission dipole) is represented by its own wobbling cone parameters (Fig. 1c), therefore an ensemble of molecules is made of emission dipole directions contained in a global aperture called ψ, oriented along ρ_{av} (we suppose here a cylindrical symmetry along the fiber axis or its perpendicular, depending on the type of label used, which is confirmed by ensemble

measurements in the cases studied in this work) (Fig. 1d). If wobbling is homogeneous (same δ for all molecules), then all pointing directions ρ of the wobbling cones will be contained in an angular extension $\Delta\rho = \psi - \delta$.

The dependence of $P(\rho, \delta)$ is depicted in Fig. 2a for different values of η, for NA = 1.3. At low numerical aperture:

$$P = \cos(2\rho).\frac{\sin\delta}{\delta}$$

P reaches its extreme values (positive or negative) at $\rho = (0°, 90°)$, which is expected since these directions are along the detected polarizations.

Note that this relation has also to be adapted in the case of high NA collection, using the appropriate expression of intensities (see above) that accounts for polarization mixing. The correction in particular applies because of out-of-plane components of the molecules' emission dipole directions. For molecules tilted out-of-plane, the estimation of their orientation if using a low NA model is thus likely to be biased, especially at narrow wobbling aperture δ and high tilt angle (Fig. 2). These molecules also suffer from a lower quality of their localization estimation, due to both loss of signal and mislocations. To limit this effect, we chose to selectively address in-plane wobbling directions. First the excitation is set at normal incidence, ensuring a low photo-selection of molecules which excitation dipoles are tilted out of the sample plane. Second a NA below total internal reflection conditions is used, ensuring a low contribution of signals coming from out-of-plane emission dipoles. Note that these precautions matter especially for narrow-wobbling angles. In the case NA = 1.3 and a wobbling angle of 40°, a bias of 20% affects P for molecules tilted by 45° out-of-plane. Nevertheless, out-of-plane angles are also producing a decrease of the total intensity I_T, which is also even more pronounced when δ is small (Fig. 2). The concerned molecules loose roughly 50% of their total intensity (Fig. 2) they can thus be easily filtered out at the reconstruction step. In practice, high tilt angles are thus less likely to be detected due to their low intensity.

The following section details how the dependence $P(\rho, \delta)$ can be used for the estimation of wobbling angle (δ) and angular extension of pointing directions ($\Delta\rho$).

Estimation of δ. An estimation of δ is possible using statistical analysis over a high number of molecules attached to biological filaments, pointing on average in the direction ρ_{av}. We suppose that δ is identical for all molecules (which is a reasonable assumption, since all molecules are attached to a given filament by the same linker). The extreme $|P|$ values ($|P|_{max}$) reached for this large collection of molecules come from those who point close to a $(0°, 90°)$ direction, which are most likely found on fibers oriented close to this direction. Under low NA conditions:

$$|P|_{max} = \frac{\sin\delta}{\delta}$$

This value can be corrected for high NA, using Fig. 2a. The observation of filaments assemblies which average pointing direction is around $(0°, 90°)$ permit therefore to estimate an upper limit for the

wobbling aperture angle. In this situation, the $P(\rho,\delta)$ dependence exhibits also its highest sensitivity to δ, permitting a quantitative estimation of an upper limit for δ. Even though this method is based on a pure statistical observation, it has proven to be robust on the protein filaments analyzed in this work, with similar values obtained (within a +/- 10° variation) for different observed fibers.

Estimation of ρ. For a low NA detection aperture, and a cone lying in the sample plane, the polarization factor P can be simply related to the cone parameters (ρ,δ), which permits to deduce a simple relation:

$$\rho = \frac{1}{2} acos(P\frac{\delta}{\sin\delta})$$

This relation means that it is possible to retrieve the wobbling pointing directions ρ, (with an ambiguity between ρ and $\pi-\rho$), from the measurement of P and the *a priori* knowledge of δ.
In the case of fibers which orientation is close to (45°, 135°), P is the most sensitive to ρ, with much less sensitivity to δ. In this case, ambiguous ρ angles can also clearly be ruled out from un-physical situations (which is less feasible for other fibers orientations). This situation allow therefore to profit from statistical analysis on a high number of molecules to give a direct access to ρ, following the relation above with a δ value preliminarily determined.
This situation also permits to quantify locally (within a portion of fiber oriented at 45°, and not from an average measurement ψ, see above) the amount of angular extent experienced by ρ values over a large number of molecules, defined as $\Delta\rho = \rho - \langle\rho\rangle$. This information can in particular be related to the heterogeneity of pointing directions in the filaments organization, at the nanometric scale.

Numerical simulation of P histograms.
In order to simulate the way histograms of P are affected by the rotational dynamics of molecules, a model has been introduced that accounts for the amount of explored angles during the time measurement T, within a wobbling angle defined by the cone of aperture δ, oriented at an angle $(\rho,\eta=0°)$ (Fig. 1b). Since rotational diffusion is supposed to take place at a faster time scale than this integration time, P histograms can be constructed based on a collection of values deduced from $P=\cos(2\rho).\frac{\sin\delta}{\delta}$ with $\rho \in \left[\rho_{av}-\left(\psi+\frac{\delta}{2}\right),\rho_{av}+\left(\psi+\frac{\delta}{2}\right)\right]$, sampled every 0.3°.

These P values are collected for wobbling pointing directions ρ that fulfil the condition that the global explored angle aperture is a known ψ value (similarly as what is measured in an ensemble measurement).

Supporting Information Note 2. Data processing algorithm

The data processing is based on a custom detection and analysis scripts written in Matlab® based on an already developed tool in the frame of a Multiple-target tracing algorithm (MTT)[5], which specificity is to be optimal in conditions where signal to noise ratios are very low, which can be the case in polarized image. This algorithm has been adapted to a split-image detection, in order to reconstruct a super resolved image of polarization factors at the nanoscale. The goal of this algorithm is to retrieve, per molecule, the position $(i_{\parallel}, i_{\perp})$, $(j_{\parallel}, j_{\perp})$, radius $(r_{\parallel}, r_{\perp})$, localization precision $(\sigma_{\parallel}, \sigma_{\perp})$ and amplitude $(\alpha_{\parallel}, \alpha_{\perp})$, which serve to calculate its polarization factor P and assign it a position. This algorithm offers advantages as compared to a pure ratiometric calculation based on image registration[6], since the paring is realized at molecular level for each dSTORM stack recorded, without any requirement of precalibration experiment which may add additional positioning errors and therefore bias in the polarization factor estimation.
The algorithm contains several sequential steps detailed below.

Detection and estimation. In all steps of the algorithm, single molecule localizations (in both ∥ and ⊥ images) are based on a first detection step which uses a Generalized likelihood ratio test (GLRT) to identify the single molecule candidates for the dSTORM image (Fig. 4a,b). This detection step uses a given fixed Gaussian shape for the theoretical PSF (radius 1.3 pixels) and a limit probability of false alarm (PFA), as detailed in the original MTT algorithm[5], which defines a threshold limit (calculated empirically based on Monte Carlo simulations) above which any signal can be statistically considered as having a different origin than noise. A value PFA ≤ 10^{-6} is set to guarantee a probability of false alarm (PFA) of less than 1 pixel per image (512 × 512 pixels), which ensures a fraction of the detected single molecules close to 100% for a signal to noise ratio (SNR) higher than 20dB[5].
After the candidates have been detected by the GLRT algorithm, the amplitude, radius and position of their Gaussian PSF are estimated on both sides (∥ and ⊥) of the image, at the subpixel scale, based on a Maximum likelihood (ML) estimation using a Gauss-Newton regression. This regression uses the GRLT obtained values of radius and position as initial parameters. The localization accuracy (σ) is estimated from a computation of the Cramer-Rao bound (CRB) limit. It has been shown in particular that the estimated precision is optimal for a SNR higher than 20 dB[5].

1- Estimation of the vector between the two (∥ and ⊥) images: association of ∥ and ⊥ emitters.
Assuming a translation between the two (∥ and ⊥) images due to their construction by the Wollaston polarization beamsplitter prism, these two images are expected to be distant by a vector which is the same for all molecules of the image. The knowledge of this vector is required for the detection of the molecule-pairs (∥ and ⊥ PSF images of each single molecule) present in a dSTORM images stack. Since the vector estimation is required with a high precision, we chose to measure this vector using the existing molecules in the image rather than with a pre-calibration, which could differ in precision. This solution is also favored as compared to image registration methods, due to their low density.
Since single molecules have different signal level in the ∥ and ⊥ sides, the localization precision on both sides can vary considerably from one molecule to another. We chose therefore to evaluate this vector over many single molecules to obtain an average which would represent the needed vector with a sufficient precision. To obtain a statistical vector estimation, we use the 100-1,000 first frames

of the dSTORM recorded stack, which is sufficient to acquire typically $\sim$ 100 vector estimations. The use of the whole dSTORM stack is also possible; however it would increase considerably the computation time with low gain in precision. Overall, the number of estimated vectors is chosen such as to ensure a precision of the vector estimation much lower than the localization precision.
In order to ensure an optimal determination of the vector for the estimation of P, appropriate statistical tests are run based on the knowledge of the localization precision estimated on both ∥ and ⊥ sides. First, to obtain the best vector candidate, the molecule-pairs representative of the most probable vector are identified. For this, all possible vectors joining two ∥ and ⊥ molecules of the images are calculated and the squared norms of the differences between all the obtained vectors are calculated (Fig. 4c). This leads to a statistical distribution, within which only the candidates which difference is below 4.2 times the obtained standard deviation are kept (pure significant test assuming that the difference between norms follows a Gaussian distribution, this value guarantees a 95% confidence level to have similar directions between the selected pairs of PSF images). Second, an additional selection is performed to determine the most optimal vector. This second step compares the obtained vector squared-norms and keeps the largest ensemble of similar squared-norms in this population. For this a sub-optimal detection is run (in order to minimize the algorithm complexity, the only hypothesis being that the error on position is Gaussian), keeping errors only below a threshold that guaranties a 95% confidence level within the obtained distribution.

2- Pairs identification. After this optimal vector is calculated, for each identified molecules on the "left" image (∥), it's "right" corresponding image (⊥) is coupled by selecting the nearest neighbor to the expected position at a vector distance from the left image, within a spatial range corresponding to the localization precision (Fig. 4d). A similar operation is performed starting from the right image, to ensure that all couples are considered. These molecules pairs are localized over the full dSTORM stack (4,000 – 80,000) (Fig. 4e). This allows a calculation of P for each molecule for the reconstruction of a polarization dSTORM image, based on the parameters position ($i_{\parallel}, i_{\perp}$), ($j_{\parallel}, j_{\perp}$), radius ($r_{\parallel}, r_{\perp}$), localization precision ($\sigma_{\parallel}, \sigma_{\perp}$) and amplitude ($\alpha_{\parallel}, \alpha_{\perp}$) (see above). The absence of neighbor molecule (Fig. 4d) leads to an estimation of the corresponding intensity that is taken as the integration over all pixels signals within a size corresponding to the radius of the present-molecule in the pair.

3- Calculation of P. The polarization factor $P = \frac{I_{\parallel} - I_{\perp}}{I_{\parallel} + I_{\perp}}$ is then calculated for each pair found, based on the integrated intensities $I_{\parallel}$ and $I_{\perp}$ which are calculated from ($\alpha_{\parallel}, r_{\parallel}$) and ($\alpha_{\perp}, r_{\perp}$):

$$I = 2\sqrt{\pi} r \alpha$$

Note that events corresponding to absent neighbor molecule (low $I_{\parallel}$ or $I_{\perp}$ intensities) are not represented in experimental histograms, even though they are detected from the polar-dSTORM algorithm. These events would indeed lead to $P \sim \pm 1$ with low confidence on P and their localization, since they correspond to very low intensity levels for one of the analyzed channel.
P is finally reported as a colored pixel which size is the sub-pixel grid chosen for the reconstruction algorithm (Fig. 4f). The final molecule position in the polar-dSTORM image is a weighted function of the positions of molecules in both ∥ and ⊥ images (($\hat{\imath}_{\parallel}, \hat{\imath}_{\perp}$),($\hat{\jmath}_{\parallel}, \hat{\jmath}_{\perp}$)), accounting for their localization precision:

$$\hat{\imath} = \frac{\sigma_{\parallel}^2 . \hat{\imath}_{\perp} + \sigma_{\perp}^2 . (\hat{\imath}_{\parallel} - v_i)}{\sigma_{\parallel}^2 + \sigma_{\perp}^2}$$

And similarly for $\hat{\jmath}$. v_i is the component of the vector along the *i* direction. Note that the precision on v_i is much higher than on $(\hat{\imath}_{\parallel}, \hat{\imath}_{\perp})$, this ensures that the final localization precision in the polar-dSTORM image is as good as the best value among $(\sigma_{\parallel}, \sigma_{\perp})$.

Postprocessing. At last, a few postprocessing steps are performed. First, low-density localizations are removed, by filtering-out events which contain below 3 localizations identified in a region of size 50 nm × 50 nm. Second, lateral drift is corrected using crosscorrelation. Sub-stack of 1,000 images are processed generating a STORM image and then performing a crosscorrelation of this image with the STORM image of the initial sub stack, resulting in a map of relative displacements along both perpendicular in-plane axes X and Y[7]. A "drift versus frame number" plot is deduced and interpolated for all the frames in each substack, and then finally used as a reference to subtract all STORM localization positions along both X and Y detections.

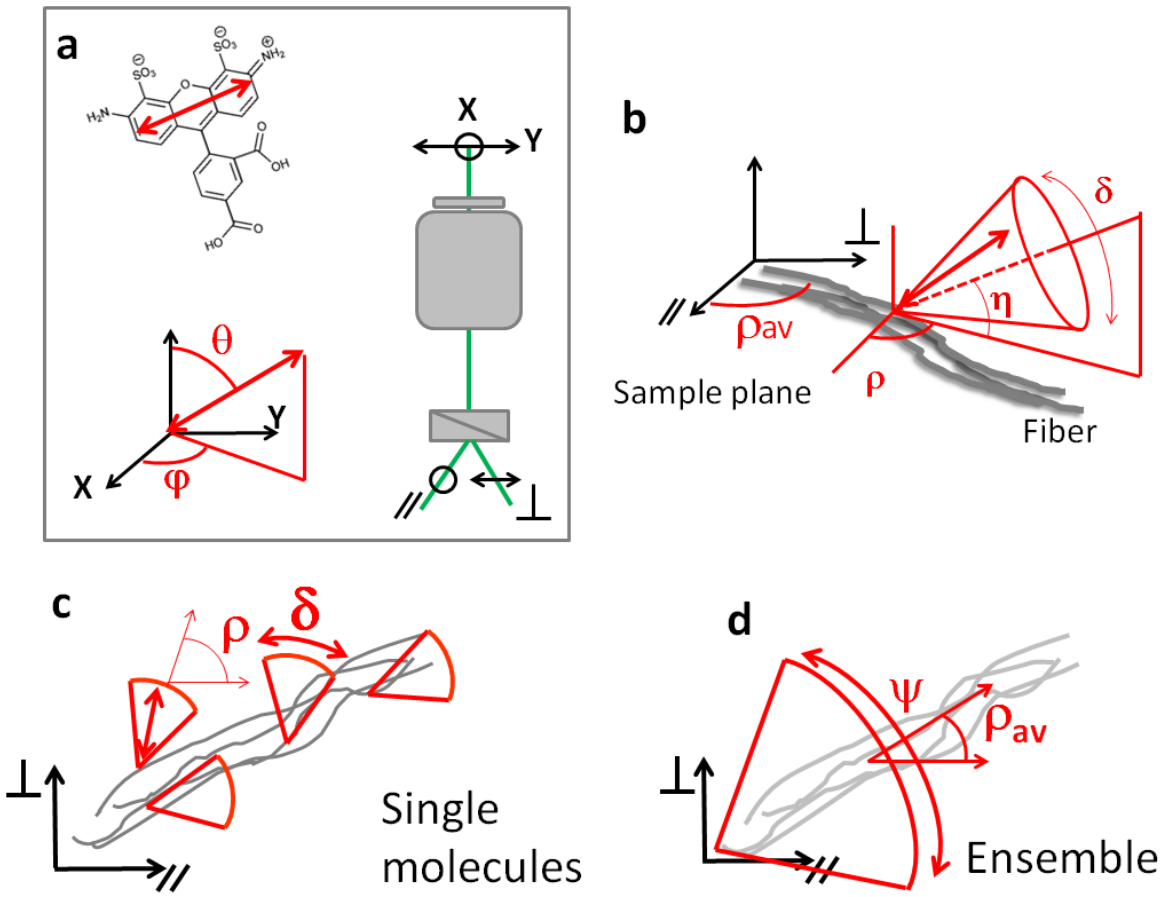

Fig. S1. Definition of angles used in the model and data analysis. (a) Single molecule orientation in the laboratory frame (X,Y,Z) (∥ and ⊥ are the measured analysis directions of polarized fluorescence intensities). The red arrow represents the emission dipole direction (here on an Alexa Fluor 488 molecule). (b) Wobbling of single molecules around a given direction (ρ, η), in an angular aperture δ. The average fiber direction is ρ_{av}. (c) Many wobbling molecules along a filamentous assembly (here a 2D representation is given). d) Equivalent picture seen by an ensemble measurement, the average direction of all molecules ρ_{av} defining also the fiber direction in the sample plane (or its perpendicular depending on the label), following an assumption of cylindrical symmetry. ψ is the global cone aperture angle encompassing all angles explored by single molecules.

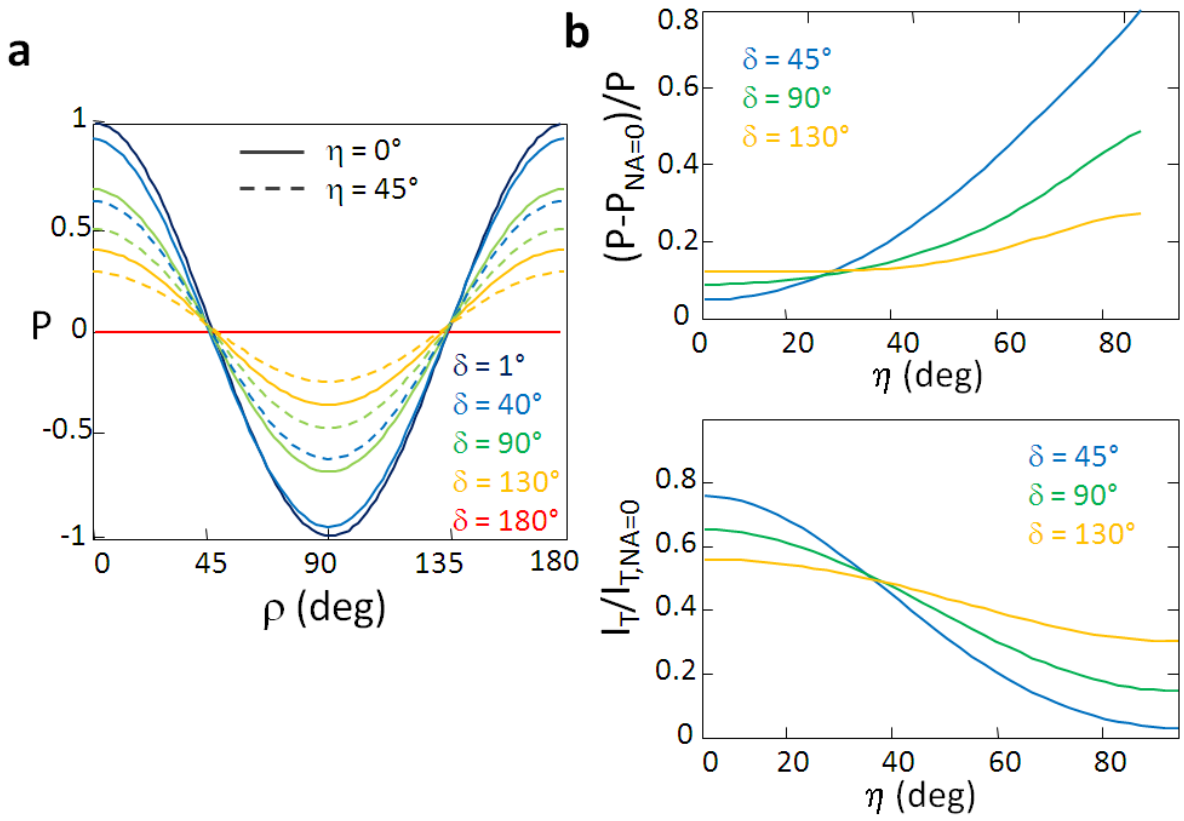

Fig. S2. Effect of high NA collection on polar-dSTORM analysis. (a) Dependence $P(\rho, \delta)$ for cone apertures δ in the smaple plane (η = 0°) and tilted (η = 45°) out-of-plane. The smallest the wobbling angle is, the largest the error on P will be for fibers oriented close to the analyzer axes (ρ = 0°, 90°). (b) Bias on P due to out-of-plane tilt angles η, for different wobbling apertures δ. The bias is stronger for small wobbling apertures, especially for $\eta > 45°$, where an error of 20% appears on P for δ = 45°. (c) Intensity loss due to out-of-plane tilt angles η. 50% losses are roughly expected for $\eta \sim 45°$. The reference intensity/P values are obtained with negligible NA collection ("NA = 0"). Note that high NA collection already induces a bias on P (which is accounted for in our analysis) and a decrease of I_T due the contribution of out-of-plane dipole radiations.

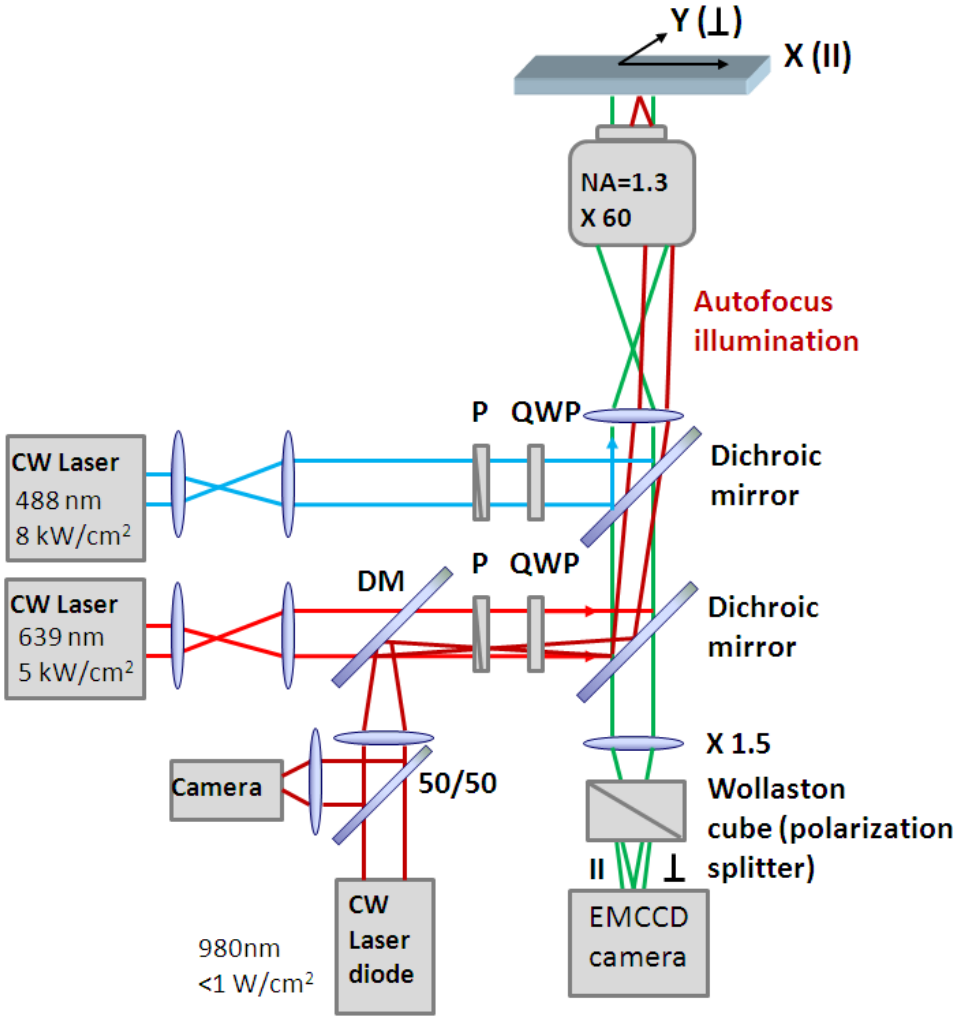

Fig. S3. Polar-dSTORM experimental set-up. (see Online Methods). The 980 nm laser is used for defocus correction in real time, the 488/639 nm lasers are used to excite the fluorescence molecules in the dSTORM mode. The Wollaston prism is used to separate the two polarized images, on two areas of the EMCCD camera. QWP: Quarter wave plates used to make the excitation polarization circular. 50/50: beamplitter. P: polarizer. DM: dichroic mirror.

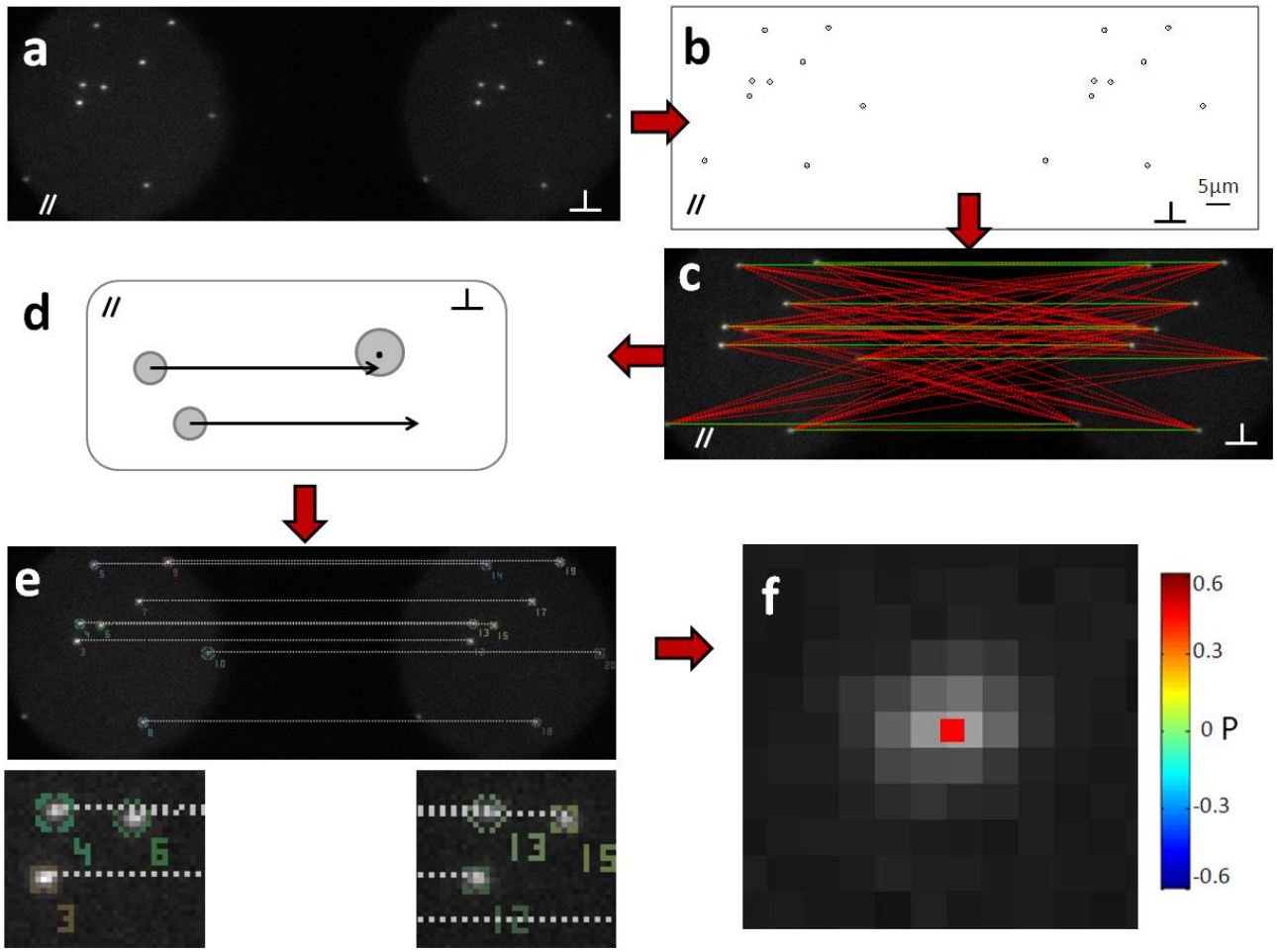

Fig. S4. **Data processing steps.** Different steps of the localization algorithm for polarization factor imaging. (a) Polarized single molecules image (here nano-beads are shown for their higher brightness). (b) Detection and localization. (c) Vectors identification, showing all selected pairs (in red the less probable vectors, in green the most probable vectors). (d) Pairs selection. Top: a case where a molecule pair is found, the vector falling within the range of its localization precision represented by the circle. Bottom: no molecule pair is found, this case leads to P ~ 1 since the associated intensity is the averaged over all noisy pixels within the size of the localization precision of the ‖ molecule. (e) Result of the final pair selection. A few detected molecule-pairs are shown. (f) Polarization factor image of a single molecule (the colored pixel has the size of the sup-pixelization chosen for the d-STORM rendering (grey background: diffraction-limited spot).

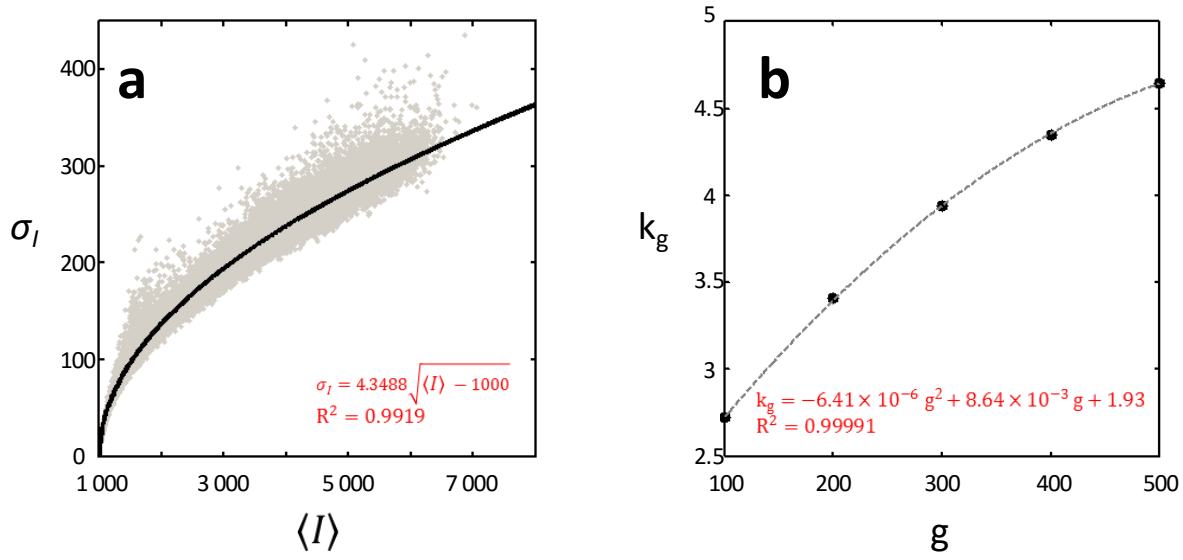

Fig. S5. Camera noise estimation and calibration. (a) Dependence between the standard deviation σ_I of the measured signal and its mean value $\langle I \rangle$, measured on 500 samples (image regions of interest), for the case g = 400. Square markers: experimental data, black line: fit using the equation $\sigma_I = k_g\sqrt{I - 1000}$, k_g = 4.3488. (b) Relationship between the noise factor *kg* and gain g. Round markers: experimental data, Dashed line: fit using a polynomial equation $k_g = ag^2 + bg + c$. Fit parameters values and quality factor are given in the graphs.

The camera calibration has been performed as follows.

Offset. In order to guarantee the precise quantitative data analysis, the response of the camera has been investigated. First, the camera response was analyzed in dark conditions showing a systematic offset of 1,000 counts, irrespectively of the gain and exposure time. This offset is subtracted from all data acquisitions, including calibrations.

Linearity. To investigate the linearity of the camera response for different acquisition settings, images of an illuminated white object (piece of paper) have been recorded under several excitation powers, between 0.5 mW and 3.5 mW, in order to produce a widespread range of signal. During each test 100 images were recorded and averaged to reduce the influence of fluctuations. For each condition, different regions of interest have been chosen, over which the response has been averaged. For this analysis, two different camera gain settings were considered (Gain=100, 300). We observed a trend on nonlinear intensity dependence for a measured signal above 60,000 counts. Measured amplitudes of single molecules PSFs should be kept below this threshold signal. Signal values below this threshold indeed clearly show a linear relationship between the recorded signal and the excitation power, which guarantees that the measurements can be analyzed with a quantitative approach.

Noise. For each case, 500 images were recorded, allowing to analyze the intensity standard deviation σ_I as a function of the mean value of the signal $\langle I \rangle$. A global analysis performed for different

configurations demonstrates that σ_I depends on the mean signal following a relation: $\sigma_I = k_g\sqrt{I - I_{offset}}$. The factor kg was found to be dependent on the gain *g* and the intensity level. The dependence of *kg* versus *g* could be written by applying polynomial fitting method: $k_g = ag^2 + bg + c$. This noise relation differs from pure Poisson noise, which is expected since the camera signal is processed after electronic magnification thus inducing electronic noise sources.

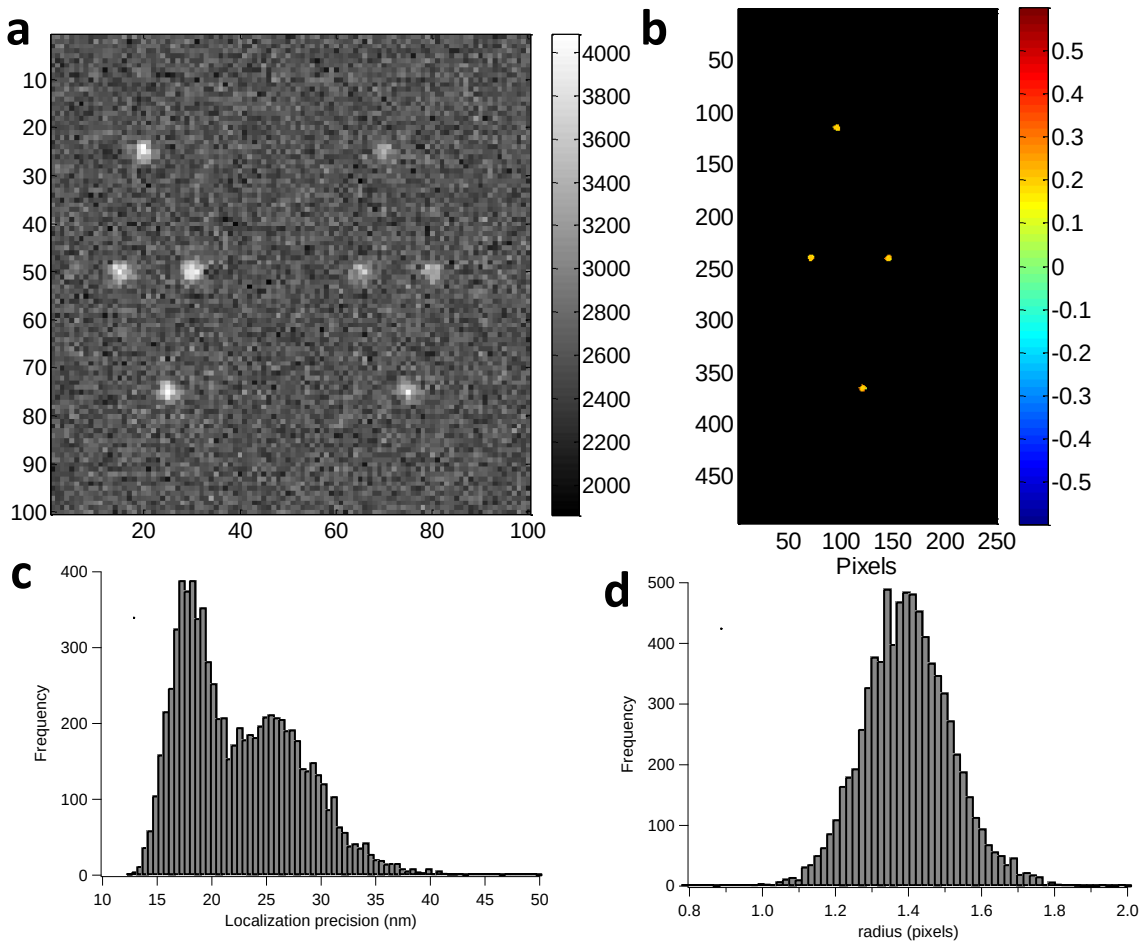

Fig. S6. **Simulations of the estimation precision/bias on P**. (a) Raw simulated STORM image. Window size = 11 pixels, PSF radius = 1.4 pixel, P = 0.2, I_T = 30,000 counts, Background (Bg) = 2,500 counts and camera gain = 500, for all molecules of the image. (b) Super-resolved image of polarization factor (sub-pixelization: pixel size /5). (c) Statistics obtained for the localization precision the PSF Gaussian fit, for 4,000 molecules. (d) Statistics obtained for the radius.

Estimation precision and bias on P. In order to observe the effect of the experimental factors and the limitations of the polar-dSTORM detection algorithm, a simulation has been implemented to generate raw polarization factor images. For each of the chosen scenario, the simulation parameters (intensity, background, PSF size) are taken from typical experimental values. The noise model is adapted based on the intensity dependent obtained from the camera calibration (see above), considering for each molecule its total intensity $I_T = I_{\parallel} + I_{\perp}$. The starting parameters are: radius of the PSF to be detected (1.4 pixels); detection window size (11x11 pixels); background intensity value (1,000 to 3,000); total intensity (I_T) (5,000 to 40,000 EMCCD counts); camera gain (300 or 500), number of frames (1,000), EMCCD offset (1,000 EMCCD counts) Probability of false alarm (PFA = 10^{-6}); frame size (100x100 pixels); number of molecules per frame (typically 4); vector length

between two split images (50 pixels). The polarization factor P varies from fixed value to random values between 1 and -1 depending on the study. The two images intensities $I_{\parallel}$ and $I_{\perp}$ are deduced from I_T and P from:

$$I_{\parallel} = I_T.\frac{1+P}{2}$$
$$I_{\perp} = I_T.\frac{1-P}{2}$$

Once the localizations and intensities lists are set, a PSF filter is created to blur the image, background is added, noise is included following the noise model developed above, and the polar-dSTORM algorithm is run.

Estimation precision on ρ. Following the relation between P and ρ (see Supplementary Note above), it is possible to evaluate numerically the estimation precision on ρ under a given experimental situation. Noise has been introduced in the ρ estimation as a standard deviation (σ_ρ) which is directly related to the standard deviation on P (σ_P) by the relation $P(\rho, \delta)$ at a given δ value. Following the simulated dependence $\sigma_P(P, I)$, an empirical relation between σ_ρ and I can be found and used to represent experimental data. In particular to represent experimental values ρ, ρ is taken as a random value contained in the range $[\hat{\rho} \pm \sigma_\rho]$, with $\hat{\rho}$ the true expected value from $P(\rho, \delta)$.

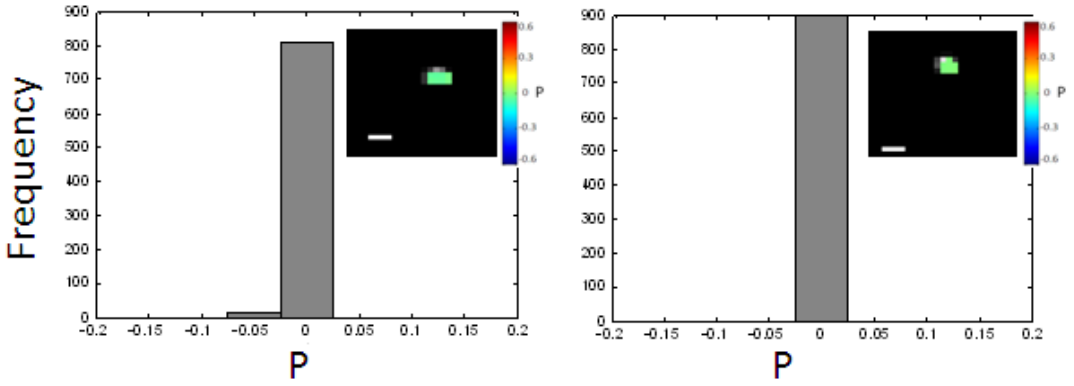

Fig. S7. **Experimental validation of the ultimate precision on P**. Polarization analysis on single fixed nano-beads (two examples). The P image is superimposed with the dSTORM image (grey). Pixel size = 53 nm (Gaussian blur = 30nm). σ_P ~ 0.005 (left, thresholding I_T = 26,000 counts) and 0.006 (right, thresholding I_T = 22,000 counts). Experimental conditions: background signal = 1,500 counts; camera gain: 1; 6,000 frames recorded. Localization precision ~ 10 nm. Scale bars, 200nm.

In order to simulate experimentally an "ideal" case in terms of noise, background and intensity, an analysis on very bright emitters of known anisotropy (nano-beads) is presented. For this experiment, blue nano-beads (Fluospheres diameter 20nm, 625-645 nm, Life Technologies) were used. The anisotropy is expected to be zero, due to the complete depolarization of the signal (the reason is the strong fluorescence resonant energy transfer between randomly oriented fluorophores embedded in the nano-beads).

The experiment was performed on fixed beads attached to the cover glass, the beads concentration was adapted to visualize only few of them (~ 4 to 30 beads in the field of view). A 20 µL droplet of ~ 10 nM of fluorescence beads was placed on a glass coverslip and allowed to evaporate slowly. Then the sample was washed two times with ddH_2O in order to remove non-fixed beads. The sample was illuminated with 639 nm wavelength at an excitation power of 0.5 mW/cm^2. For the used experimental conditions and an intensity thresholding of about 20,000 counts, the precision obtained on P is σ_P ~ 0.005. Note that this low value is partly accessed because the gain is set to a very low value. Similar results of intensity measured at a gain of 300 would lead to twice the standard deviation: σ_P ~ 0.01. This value is the lowest measured precision on an experimental image of P, and gives therefore an estimation of the sensitivity of the technique.

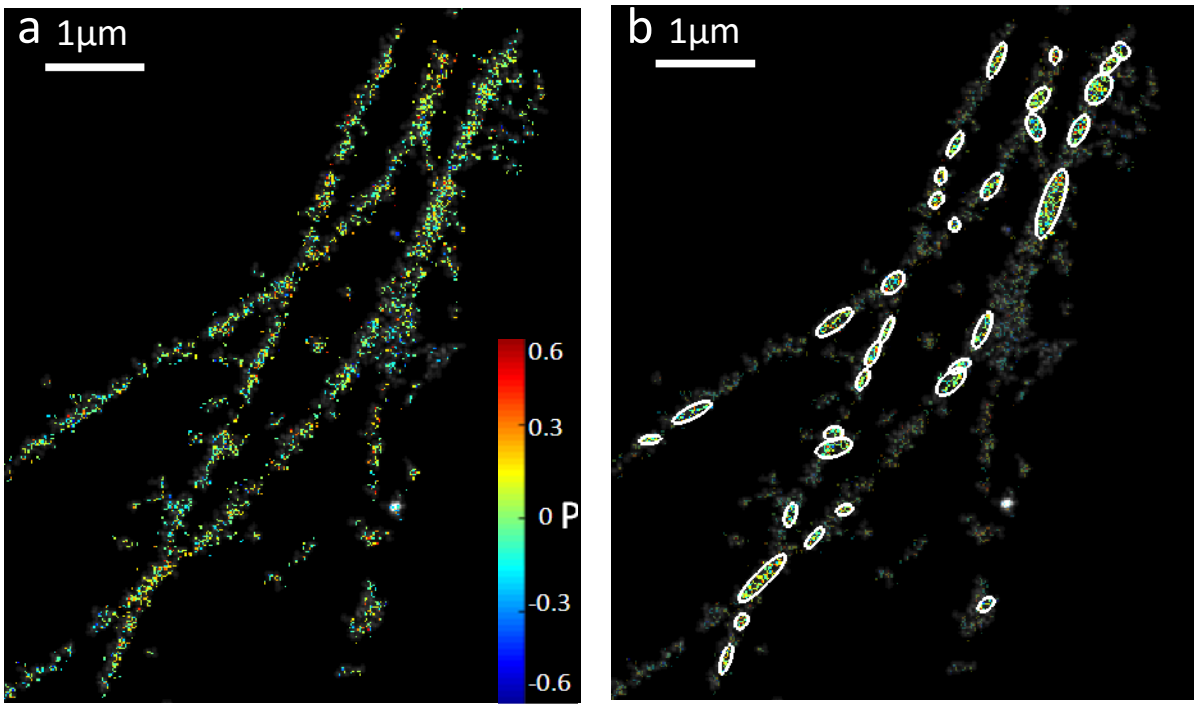

Fig. S8. **Fiber orientation estimation.** Automatic cluster selection (Sample: microtubules in a COS 7 cell labeled with Alexa Fluor 647). (a) Full super-resolved polarization factor image. (b) Clusters selected from the automatic selection cluster algorithm (connectivity: 8). Regions selected are surrounded by a white ellipse.

In order to retrieve the local orientation of fibers sub-regions in a reconstructed super resolved image, an analysis based on a "cluster" of localizations is performed using the Matlab® Image Processing Toolbox. Being able to identify clusters with a clear orientation (ρ angle) allows retrieval of averaged molecular order information (δ), as well as statistical analysis over several regions of the sample. A super resolved image is converted into a binary image, in which a cluster selection is performed based on the connectivity between sub-pixels (considering 8 neighbors in all directions). The program identifies groups of connected sub-pixels, which define fiber sub-regions. To obtain the local orientation of a fiber sub-region, an ellipse is defined surrounding the cluster region, which major axis orientation relative to the horizontal axis X is assigned to be the averaged angle ρ.

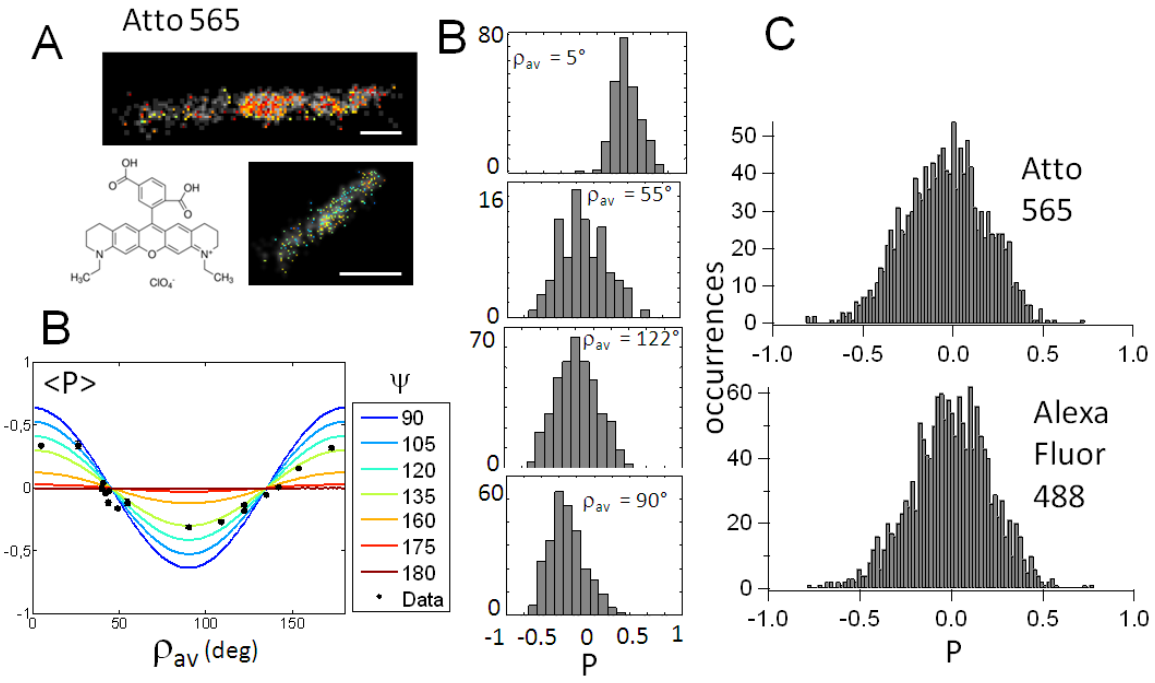

Fig. S9. **Polar-dSTORM imaging in actin stress fibers labeled with Atto 565**. (A) Atto 565 molecular structure and P images (superimposed to traditional dSTORM images, grey scale) of local regions in phalloidin labelled actin stress fibers in fixed cells. Intensity threshold: 50,000 counts, expected σ_P < 0.05. Scale bars, 200 nm. Gaussian blurring size: 25 nm. (B) P histograms for different portions of fibers and averaged behaviors reported in the ⟨P⟩(ρ_av,ψ) dependence. An average molecular order ψ ~ 130° is obtained, while the analysis of individual histograms shows a wobbling extent of about δ ~ 80°. (C) Global P histograms for actin stress fibers or orientation ρ_av close to 45°. Atto 565 (above, 1527 molecules) and Alexa Fluor 488 (below, 1344 molecules). The histogram widths are very close to each other (standard deviation Atto 565: 0.22; Alexa Fluor 488: 0.17), confirming that the wobbling extent of both fluorophores are close.

For this comparative study, both Alexa Fluor 488 and Atto 565 phalloidin staining are done in same conditions. Briefly, COS 7 cells were grown in DMEM, plated on 20 mm diameter #1.5 cleaned coverslips coated 24 hours with fetal bovine serum, in 12-well flat bottom cell culture plate (Corning) for 24 hours. Cells were first washed with pre-warmed PBS. They were fixed and permeabilized for 1-2 min using 400 µl of 0.3% (v/v) glutaraldehyde (EM grade, Electron Microscopy Sciences) and 0.25% (v/v) Triton X-100 in PBS, then post-fixed again using 400 µl of 2% (v/v) glutaraldehyde in PBS for 10 min. The sample was treated with freshly prepared 0.1% (w/v) sodium borohydride (NaBH4, Sigma) in PBS for 7 min to reduce background fluorescence of glutaraldehyde. Cells were washed three times 10 min in PBS. Actin filaments were labelled with 300 to 500 nM Alexa Fluor 488-phalloidin (Life Technologies) or Atto 565-phalloidin (Atto Tec) for overnight incubation at 4°C in the dark. The sample was then briefly washed with PBS and the coverslip was mounted for STORM imaging on a slide with a cuvette filled with STORM buffer, and sealed with Picodent Twinsil than nail polish. The

STORM buffer was made of 50 mM β mercaptoethylamine (MEA, Sigma-Aldrich) and an oxygen scavenger as followed: 0.5 mg/ml glucose oxidase (G0543, Sigma-Aldrich), 40 μg/ml catalase (C40, Sigma-Aldrich) and 10% (w/v) glucose dissolved in a buffer consisting of 100 mM Tris-HCl (Sigma-Aldrich) plus, for Atto 565-phalloidin only, 1 mM ascorbic acid (Sigma-Aldrich) and 1 mM methyl viologen (Sigma-Aldrich)). The pH of the final solution was adjusted to 7.5-8.

To image Atto 565 molecules, the set-up was kept unchanged except for a different excitation source (561nm Sapphire, Coherent Santa Clara CA) at 5 kW/cm^2 intensity at the sample plane, with appropriate optical dichroic and emission filters (beamsplitter HC BS 573, Semrock Rochester NY and 590/50 bandpass filter, Chroma Technology Bellows Falls VT). The calibration of polarization factors was also adapted for this specific wavelength.

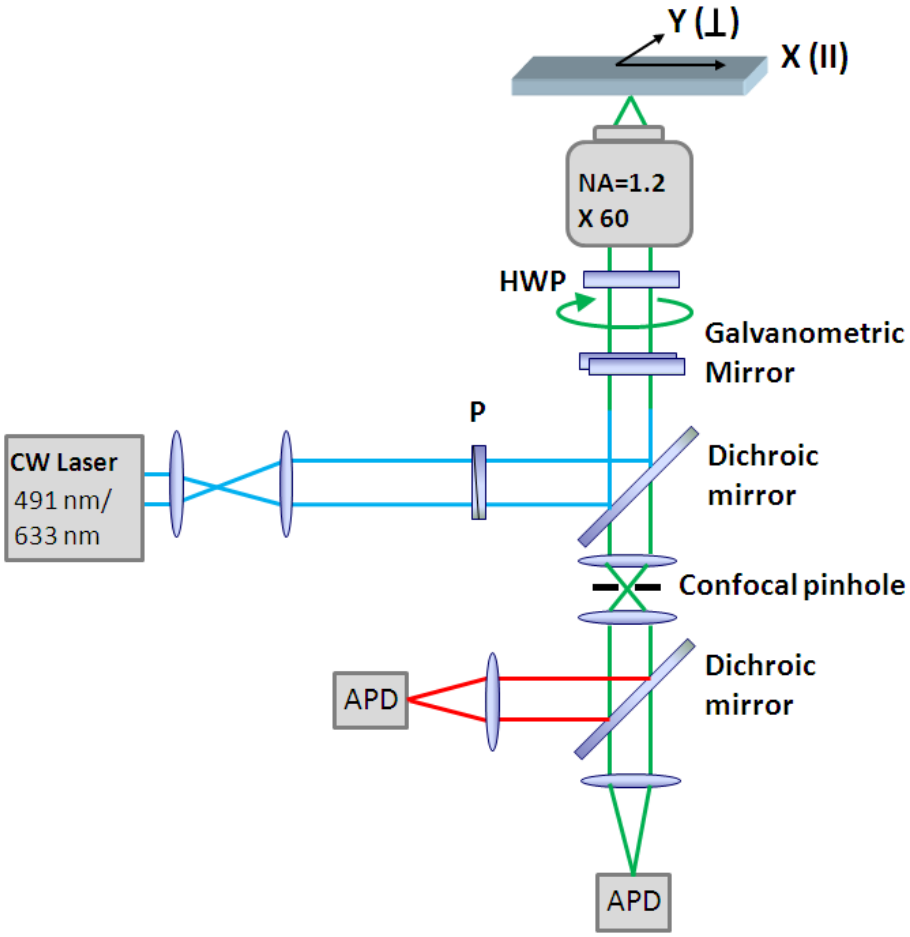

Fig. S10. **Polarization-resolved confocal microscopy set-up**. Experimental set-up for confocal polarization resolved fluorescence (see Online Methods). HWP: Half wave plate mounted on a rotation motor. P: polarizer. APD : Avalanche Photodiode.

Supporting Information References

1. Cantor CR, Schimmel PR, *Biophysical Chemistry. Part II: Techniques for the Study of Biological Structure and Function*.

2. Forkey JN, Quinlan ME, Goldman YE (2000) Protein structural dynamics by single-molecule fluorescence polarization. *Prog. Biophys. Mol. Biol.* 74: 1–35.

3. Brasselet S (2011) Polarization-resolved nonlinear microscopy: application to structural molecular and biological imaging. *Adv. Opt. Photonics* 3: 205.

4. Axelrod D (1979) Carbocyanine dye orientation in red cell membrane studied by microscopic fluorescence polarization. *Biophys. J.* 26:557–573.

5. Sergé A, Bertaux N, Rigneault H, Marguet D (2008) Dynamic multiple-target tracing to probe spatiotemporal cartography of cell membranes. *Nat. Methods* 5:687–694.

6. Gould TJ et al. (2008) Nanoscale imaging of molecular positions and anisotropies. *Nat. Methods* 5:1027–1030.

7. Guizar-Sicairos M, Thurman ST, Fienup JR (2008) Efficient subpixel image registration algorithms. *Opt. Lett.* 33:156–158.